2005 WSEAS Int. Conf. on ENVIRONMENT, ECOSYSTEMS and DEVELOPMENT, Venice, Italy, November 2-4, 2005 (pp249-254)

The optimum wavelet-based fusion method for urban area mapping

S. IOANNIDOU†, V. KARATHANASSI†, A. SARRIS*

†Laboratory of Remote Sensing
School of Rural and Surveying Engineering
National Technical University of Athens
9 Iroon Polytechneiou Street, 157 80, Zographos
*Laboratory of Geophysical - Satellite Remote Sensing & Archaeo-environment
Foundation for Research & Technology (F.O.R.T.H.), Hellas, Institute for Mediterranean Studies
Melissinou & Nik. Foka 130, PO. Box 119, Rethymnon 74100, Crete
GREECE
si01613@survey.ntua.gr, karathan@survey.ntua.gr, asaris@ret.forthnet.gr

Abstract: - In this paper we examine the comparative use of different types of wavelets for Quickbird multisensor image fusion, for the purposes of high-resolution urban mapping. Based on the Discrete Wavelet Transform, several types of standard wavelets were implemented and evaluated. The best wavelet fusion results were combined with the IHS image fusion method using two types of colour composites. The IHS image fusion method was also implemented. The crossbred wavelet and IHS transform provides the most accurate colour representation of the spectral information of the initial bands, improving also their spatial resolution. Based on the results of the evaluation, a high-resolution fusion-based map of Heraclion, Crete was produced.

Key-Words: - Multisensor image fusion, High resolution mapping, Wavelets, IHS transform

1. Introduction

Multisensor image fusion is a technique leading to the increase of the spatial resolution of low detail multisensor acquired images, preserving their spectral information. Military, medical imaging, computer vision, robotic industry and remote sensing are some of the fields benefiting from image fusion [3].

In this paper, investigation of image fusion techniques for producing background information of urban maps, scale 1:10.000, is undertaken. For this purpose, secondary information is provided by High Resolution Remotely Sensed (HRRS) fused data and primary information, like main road network etc., is extracted from initial HRRS data topographic maps.

In general, image fusion techniques can be grouped into two classes [8]: colour related (e.g. IHS transform) and numerical (e.g. Wavelets). In this study we examine and evaluate the use of wavelets and colour related techniques for Quickbird image fusion, to produce a high-resolution digital map.

2. Wavelet analysis and image fusion

2.1. Basic aspects of wavelet-related theory

The wavelet transform ([2], [5]) aims in both multitemporal and multiscale pyramid structured signal analysis, similar to a Laplacian pyramid pattern. It uses non-correlated orthonormal basis functions called wavelets, providing both time and scale representation, adaptable to every signal.

For the typical wavelet transform, an expansion set is defined for any signal f(t):

$$f(t) = \sum_m \sum_n c_{m,n} \psi_{m,n}(t) \qquad (1)$$

where both m and n are integer indices and $\psi_{m,n}(t)$ represents successive scaled and dilated versions of a single wavelet function $\psi(t)$, called mother wavelet. The wavelet basis functions are extracted from a mother wavelet function as follows [1]:

$$\psi_{m,n}(t) = 2^{-m/2} \psi\left(2^{-m} t - n\right) \qquad (2)$$

The factor $2^{-m/2}$ maintains a constant norm for the wavelet basis independent from scale m and suggests that throughout wavelet scaling and dilations successive partitioning of the signal's spectrum occurs.

For an iterated wavelet transform, additional real-valued coefficients $\alpha_{m,n}$ are required. At each scale, $\alpha_{m,n}$ and $\alpha_{m-1,n}$ denote scaled versions of f(t) at resolutions 2^m and 2^{m-1} respectively. So, a signal can be expressed in a multiresolution basis as

a linear combination of wavelet and scaling coefficients $c_{m,n}$ and $\alpha_{m,n}$ respectively [1].

The approximation and wavelet coefficients $c_{m,n}$ and $\alpha_{m,n}$ can be obtained by [7]:

$$\alpha_{m,n}(t) = \sum_k h_{2n-k}\alpha_{m-1,k} \quad (3)$$

$$c_{m,n}(t) = \sum_k g_{2n-k}c_{m-1,k} \quad (4)$$

where h and g are lowpass FIR and highpass FIR filters respectively.

The initial signal can be reconstructed implementing the inverse DWT out of calculated wavelet and scaling coefficients.

For the 2-D DWT separate horizontal and vertical image filtering and downsampling is needed. The 2-D DWT produces four subbands at each level of analysis. The first is the scalage of the input image and the remaining three are the detail coefficients at the horizontal, vertical and diagonal directions respectively.

2.2. Wavelet image fusion

2.2.1. Pre-processing

Pre-processing of the input images includes tasks like registration and resampling.

If satellite images are taken from the same sensor at the same time (as in Quickbird imagery), no registration is needed. Each level of wavelet analysis produces an image with half the spatial resolution of the initial one. For wavelet fusion, the ratio of the resolutions of the input images must be a power of two. Quickbird imagery meet this requirement, since the proportion between the spatial resolutions of the satellite's multispectral and panchromatic sensor is 2^2 (i.e. 2.8m and 0.7m respectively) [3]. So, no resampling is needed.

2.2.2. Wavelet fusion algorithm

At first, the forward DWT is calculated for each of the input images and wavelet and scaling coefficients are extracted. The actual fusion procedure occurs during the implementation of the coefficient combination rules. The combination schemes set the necessary standards for the wavelet and scaling coefficients to be used. Rules such as the maximum absolute value between corresponding coefficients are used in latest wavelet fusion software packages [9]. Finally, the inverse DWT is calculated and the final fused image is extracted.

2.3. IHS fusion algorithm

The IHS (Intensity-Hue-Saturation) colour model simulates the human visual colour transform aims in separating the geometric information (lying in the Intensity layer) from the spectral information (included in both Hue and Saturation levels).

The image fusion algorithm first generates the forward IHS transform from a multispectral RGB colour composite and excludes the Intensity layer. Then it replaces the Intensity layer with the panchromatic image and performs the inverse IHS colour transform.

2.4. Crossbred wavelet and IHS fusion algorithm

The crossbred wavelet and IHS fusion method implements a forward IHS transform to a true-colour or near-infrared multispectral composite. In each of the cases, the intensity layer is extracted and wavelet-fused with the high resolution panchromatic image. The intensity layer is replaced by the fusion product and an inverse IHS colour transform is performed. The acquired fused image has its spatial resolution improved, having preserved its spectral characteristics.

3. Implementation

The 2-D DWT, the IHS transform and a crossbred wavelet-IHS transform were implemented to multispectral and panchromatic Quickbird imagery of Heraclion, Crete (Greece). The dataset consists of two sets of images, the first representing a peri-urban area and the second picturing an offshore urban one.

Since the spatial resolution of Quickbird panchromatic imagery is four times the spatial resolution of respective multispectral imagery, three levels of wavelet analysis are needed. The wavelet fusion algorithm was implemented between each pair of a multispectral and panchromatic image and a colour composite of fused multispectral bands was formed at the end. The selected fusion rule combines the scaling coefficients of the multispectral bands with the wavelet coefficients of the panchromatic image.

All computations were performed on a Pentium 4, 3.00GHz PC, running Windows 2000. All coefficients were extracted from the Matlab wavelet toolbox [6] and the wavelet fusion algorithm was

implemented using Oliver Rockinger's Image Fusion Toolbox [9].

Different types of standard wavelets were tried out. Since each family of wavelets consists of several different representatives (only the Discrete Meyer wavelet is unique), a very important task has been a selection procedure defining the appropriate wavelet filter size.

The selection between different types of wavelets was based on the existence of the DWT and the filter size, which was selected so that the resulting fused image would appear a close-to-canonical histogram. Finally, it was desirable to keep filter frequency response close to ideal.

To define an adequate wavelet filter length, several fused multispectral and panchromatic Quickbird images were produced using wavelets of various sizes (1^{st}, 4^{th}, 5^{th}, 6^{th}, 8^{th}, 9^{th}, 10^{th}, 12^{th} and 20^{th} class), belonging to the Daubechies family. The resulting images were photointerpreted and differences in colour, edge and shadow attribution were marked.

Photointerpretation resulted that 5^{th} (10 coefficients) and 8^{th} (16 coefficients) class Daubechies wavelets best reproduce spectral information. Out of the two, only the first one has frequency response close to ideal [4].

Wavelets satisfying all mentioned conditions are the 5^{th} class Daubechies wavelet (10 coefficients), the 5^{th} class Symlet (10 coefficients) the 2^{nd} class Coiflet (12 coefficients) the Biorthogonal Spline 4.4 (9 and 7 coefficients for the analysis and 7 for the synthesis filters) and the Reverse Biorthogonal Spline 4.4 (9 coefficients for the analysis and 7 for the synthesis filters). Although the Discrete Meyer wavelet (102 coefficients) does not meet the compact support requirement, it was implemented so as to accent the importance of the property. Wavelet fusion results for each of the cases selected are presented in Fig.1. The classic IHS fusion algorithm and the crossbred wavelet and IHS transform (using a true and a near infrared colour composite) were also implemented for both cases (Fig.5 and 6).

(a) **(b)**

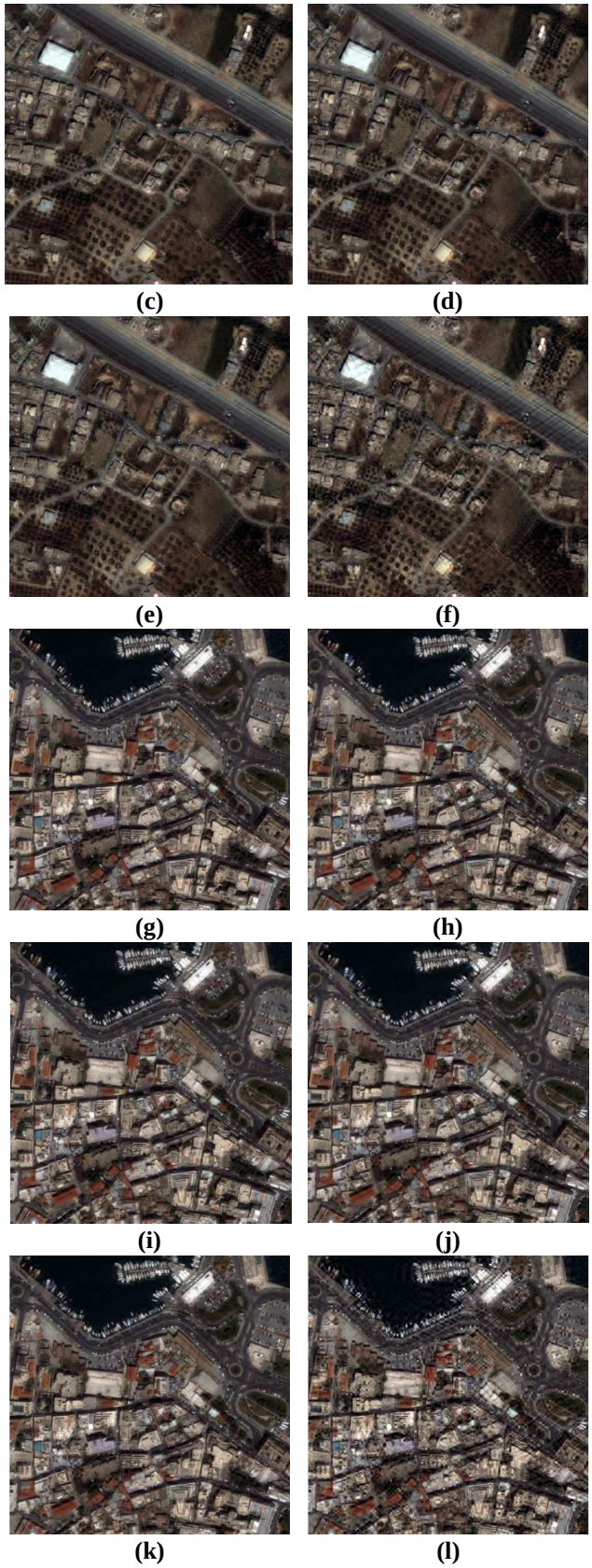

(c) **(d)** **(e)** **(f)** **(g)** **(h)** **(i)** **(j)** **(k)** **(l)**

Fig. 1. Colour composites of Quickbird peri-urban and offshore urban imagery, implementing **(a)**, **(g)** 5^{th} Daubechies, **(b)**, **(h)** 5^{th} Symlet **(c)**, **(i)** 2^{nd} Coiflet, **(d)**, **(j)** Biorthogonal Spline 4.4, **(e)**, **(k)** Reverse Biorthogonal Spline 4.4 and **(f)**, **(l)** Meyer wavelet

(a) **(b)**

Fig. 2. Colour composites of **(a)** peri-urban and **(b)** offshore urban Quickbird imagery, implementing the IHS transform

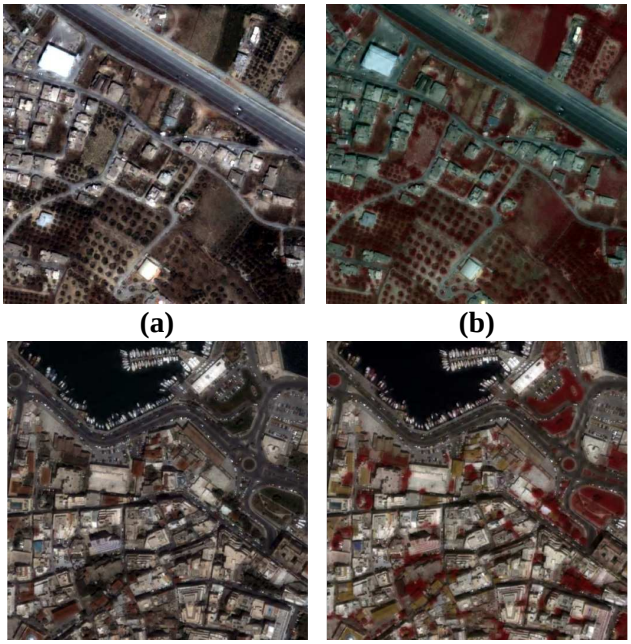

(a) **(b)**

(c) **(d)**

Fig. 3. True and near infrared colour composites of fused **(a)**, **(b)** peri-urban and **(c)**, **(d)** offshore urban Quickbird imagery, implementing wavelet-IHS transform

4. Evaluation

Two evaluations took place, the first for various wavelet-fused results (Table 1) and the second for fusion different methods (Table 2).

The best wavelet for each dataset was used in the crossbred wavelet-IHS transform.

Three types of evaluation indices were used. The 2-D correlation [6], the Peak Signal to Noise Ratio (PSNR) [11] and the SSIM quality index [10].

4.1. First evaluation

Correlation Index (multispectral bands)						
Image 1						
Band	**db5**	**sym5**	**bio44**	**rbio44**	**coif2**	**dmey**
B	0.911	0.912	0.910	0.911	**0.913**	0.911
G	0.928	0.928	0.927	0.927	**0.929**	0.927
R	0.936	0.937	0.935	0.935	**0.938**	0.936
NIR	**0.915**	0.914	0.913	0.913	0.914	0.914
Image 2						
B	0.919	**0.920**	0.918	0.918	0.919	0.919
G	0.933	**0.933**	0.932	0.932	0.933	0.932
R	0.938	**0.939**	0.938	0.938	0.938	0.937
NIR	0.946	0.946	0.946	0.946	**0.947**	0.945
Correlation Index (panchromatic bands)						
Image 1						
Band	**db5**	**sym5**	**bio44**	**rbio44**	**coif2**	**dmey**
B	0.830	0.831	**0.833**	0.827	0.831	0.830
G	0.853	0.853	**0.856**	0.855	0.853	0.854
R	0.854	0.854	**0.857**	0.856	0.854	0.855
NIR	0.690	0.690	**0.695**	0.694	0.692	0.690
Image 2						
B	0.921	0.921	**0.922**	0.919	0.921	0.921
G	0.944	0.944	**0.945**	0.944	0.944	0.944
R	0.932	0.932	**0.933**	0.931	0.932	0.932
NIR	0.880	0.880	**0.881**	0.878	0.879	0.880
PSNR Index (multispectral bands)						
Image 1						
Band	**db5**	**sym5**	**bio44**	**rbio44**	**coif2**	**dmey**
B	50.120	50.430	50.597	**51.131**	50.964	50.355
G	51.264	51.522	51.627	51.627	**52.153**	51.247
R	**54.528**	54.284	54.477	54.477	52.206	54.140
NIR	**51.160**	50.675	50.635	50.635	50.773	50.828
Image 2						
B	51.350	50.859	50.633	50.470	51.203	**51.794**
G	52.909	52.394	52.227	52.394	52.570	**53.052**
R	53.404	53.377	53.301	53.389	**53.684**	53.612
NIR	55.157	54.594	54.643	54.762	**55.181**	55.018
SSIM Index (multispectral bands)						
Image 1						
Band	**db5**	**sym5**	**bio44**	**rbio44**	**coif2**	**dmey**
B	0.481	0.481	0.481	0.476	**0.483**	0.478
G	0.531	0.532	0.531	0.531	**0.534**	0.527
R	0.577	0.578	0.578	0.578	**0.580**	0.574
NIR	0.606	0.607	0.606	0.606	**0.607**	0.604
Image 2						
B	0.483	**0.484**	0.483	0.479	0.483	0.479
G	0.509	**0.511**	0.509	0.511	0.509	0.504
R	0.521	**0.523**	0.521	0.518	0.522	0.516
NIR	0.565	**0.567**	0.566	0.562	0.567	0.561

Table 1. Correlation, PSNR and SSIM indices between fused and original bands, implementing various wavelets

4.2. Second evaluation

Correlation index (multispectral bands)				
Image 1				
Band	**Coiflet**	**321 WIHS**	**432 WIHS**	**IHS**
B	0.913	**0.926**	-	0.826
G	0.929	**0.934**	0.918	0.831
R	0.938	**0.938**	0.898	0.789
NIR	**0.914**	-	0.812	-
Image 2				
Band	**Symlet**	**321 WIHS**	**432 WIHS**	**IHS**
B	**0.920**	-0.092	-	0.880
G	**0.933**	-0.059	0.930	0.885
R	**0.939**	0.945	0.912	0.877
NIR	**0.947**	-	0.903	-
Correlation index (panchromatic bands)				
Image 1				
Band	**Coiflet**	**321 WIHS**	**432 WIHS**	**IHS**
B	0.831	0.734	-	**0.947**
G	0.853	0.808	0.845	**0.979**
R	0.854	0.847	0.706	**0.997**
NIR	0.692	-	**0.713**	-
Image 2				
Band	**Symlet**	**321 WIHS**	**432 WIHS**	**IHS**
B	0.921	0.790	-	**0.971**
G	0.944	0.759	0.831	**0.985**
R	0.932	0.902	0.827	**0.999**
NIR	0.880	-	**0.912**	-
PSNR index (multispectral bands)				
Image 1				
Band	**Coiflet**	**321 WIHS**	**432 WIHS**	**IHS**
B	50.964	**51.038**	-	27.894
G	**52.153**	50.846	46.390	27.573
R	**52.206**	49.721	32.133	27.283
NIR	**50.773**	-	36.762	-
Image 2				
Band	**Symlet**	**321 WIHS**	**432 WIHS**	**IHS**
B	**50.859**	29.678	-	26.073
G	**52.394**	29.964	36.352	26.175
R	**53.377**	50.177	36.805	26.215
NIR	**54.594**	-	37.978	-
SSIM index (multispectral bands)				
Image 1				
Band	**Coiflet**	**321 WIHS**	**432 WIHS**	**IHS**
B	0.483	0.594	-	**0.637**
G	0.534	0.599	0.516	**0.628**
R	0.580	0.563	**0.670**	0.575
NIR	**0.607**	-	0.393	-
Image 2				
Band	**Symlet**	**321 WIHS**	**432 WIHS**	**IHS**
B	0.484	0.245	-	**0.544**
G	0.511	0.209	**0.667**	0.547
R	0.523	0.587	**0.655**	0.527
NIR	0.567	-	**0.592**	-

Table 2. Correlation, PSNR and SSIM indices between fused and original multispectral bands, implementing different image fusion methods

Method	
Image 1	**Image 2**
WIHS 321	WIHS 432
Classic IHS	Symlet
Coiflet	Classic IHS
WIHS 432	WIHS 321

Table 3. Final evaluation table using different types of fusion methods sorted from best to worst (top to bottom)

5. High-resolution mapping

Based on the concepts of Quickbird image fusion and the previous results, a high-resolution digital map of Heraclion, Crete was produced.

At first, the initial multispectral and panchromatic bands were orthorectified and geo-referenced to the EGSA87 (Hellenic Geodetic Reference System) projection using a Digital Elevation Model and 30 Ground Control Points. The final multispectral and panchromatic Quickbird channels were fused implementing the crossbred wavelet-IHS transform using a true colour composite basis.

The initial images and topographic maps were used as digitization background for the extraction of eight levels of information (three categories of road network, road names, places of interest, parking areas, public services, and churches) and the creation of the digital map (Fig.4).

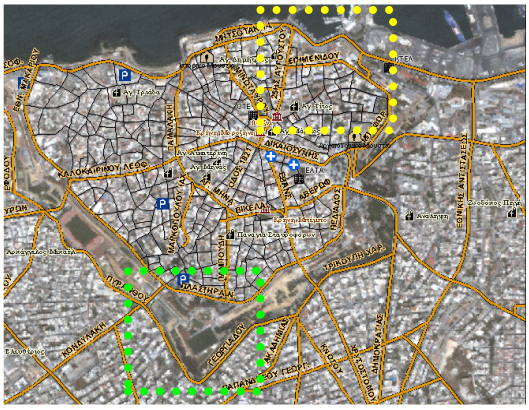

Fig. 4. Final digital map of Heraclion, Crete

6. Conclusions

When the panchromatic band is not highly correlated (0.73379 – 0.84663 for the first set of images and 0.75924 – 0.90234 for the second set of images) to the multispectral bands, the radiometric distortion produced by the IHS fusion algorithm onto a true colour composite is quite obvious.

Planning of adequate analysis levels following image scaling overcomes defects resulting from the implementation of the DWT. The multiresolution analysis image model also eliminates the impact of possible initial data noise on the fusion product.

As the wavelet filter length grows, more shadows appear in the fused image and curves become more ambiguous. Compact supportability is of major importance as far as edge attribution is concerned. The combined use of the DWT and the IHS colour model adds up to the fusion algorithm accuracy and colour attribution.

Wavelets proved to be more effective for multispectral and panchromatic Quickbird fusion purposes are the 2nd order Coiflet (for the peri-urban image) and the 5th order Symlet (as far as the offshore urban image is concerned). Both wavelets satisfy the orthogonality condition.

Studying the two dimensional correlation index results, biorthogonal wavelets tend to attribute best the initial panchromatic spatial information (values range from 0.69480 to 0.85742 for the first set of images and from 0.88089 to 0.94514 for the second set of images), compared to other types of wavelets.

The best fusion method for the peri-urban image is the simple DWT or the crossbred wavelet-IHS transform, using a visible colour composite. The fusion method proved to give better results for the offshore urban area is the simple DWT (with correlation indices from 0.91996 to 0.94653 and PSNR indices from 50.85900 to 54.59400), or the crossbred wavelet and IHS transform using a near infrared colour composite. The combination of IHS and wavelet fusion methods improves the quality of the results given by each of the methods separately.

7. Acknowledgements

This study was carried out within the framework of the project “Development of an Expert System for the Monitoring, Management and protection of the Natural Landscape and Environmental Resources of the island of Crete” (CRINNO-Crete Innovative Region – EMERIC I)”, which is funded by the Region of Crete and the European Union.

References:

[1] Burrus C.S., Gopinath R.A., Guo H., *Introduction to wavelets and wavelet transforms,* Prentice-hall Inc, New jersey, 1998.

[2] Daubechies I., *Ten lectures on wavelets*. 3rd printing, CBMS, SIAM (Society for Industrial and Applied Mathematics), Philadelphia, Pennsylvania, USA, Vol.61, pp.194-202, 1994.

[3] Gungor O., Shan J., Evaluation of satellite image fusion using wavelet transform. *Proceedings of the ISPRS, commission VII, WG III/6, Istanbul,* 2004, published on CD-ROM, paper n° 236.

[4] Lingsong H., Tat T.W., 2004, The DSP class. (Url:http://heliso.tripod.com/java_hls/lesson0_e.html).

[5] Mallat G.S., A theory for multiresolution signal decomposition: the wavelet representation. *IEEE transactions of pattern analysis and machine intelligence,* Vol.11, No.7, 1989, pp.674-693.

[6] Misiti M., Misiti Y., Oppenheim G., Poggi J.M., *Wavelet toolbox for use with MATLAB: User’s guide,* The mathworks Inc, Natick, NA, 2004.

[7] Nikolov S., Hill P., Bull D., Canagarajah N., Wavelets for image fusion. *Wavelets in signal and image analysis, from theory to practice,* Kluwer academic publishers, Netherlands, Editors: Petrosian A.A. and Meyer F.G., 2001, pp.213-239.

[8] Pohl C., Genderen J.L. Van., Multisensor image fusion in remote sensing: concepts, methods and applications. *International journal of remote sensing,* Vol.19, No.5, 1998, pp.823-854.

[9] Rockinger O., Pixel-level fusion of image sequences using wavelet frames. *Proceedings of the 16th Leeds annual statistical research workshop, Leeds University Press,* 1996, pp.149-154.

[10] Wang Z., Bovik A.C., Sheikh H.R., Simoncelli E.P., Image quality assessment: from error visibility to structural similarity. *IEEE transactions on image processing, April 2004,* Vol.13, No.4, 2004, pp.600-612.

[11] Wang Z., Sheikh H.R., Bovik A.C., Objective video quality assessment. *The handbook of video databases: design and applications,* Chapter 41, Editors B. Furht and O. Marqure, September 2003, CRC press, 2003, pp. 1041-1078.